IL NUOVO CIMENTO **48 C** (2025) 64
DOI 10.1393/ncc/i2025-25064-7

COLLOQUIA: IWM-EC 2024

Constraints on the nuclear EOS from heavy-ion collision simulations

M. COLONNA and the TMEP COLLABORATION
INFN, Laboratori Nazionali del Sud - Catania, Italy

received 26 November 2024

Summary. — Within the transport model evaluation project (TMEP) of simulations for heavy-ion collisions, we present a detailed study of the performance of different transport models for mean-field propagation in a box and in Sn+Sn collisions at 270 AMeV, with particular emphasis on the production of pions and Δ resonances, which are often employed as probes of the nuclear symmetry energy. Thus, we prescribe common and rather simple physics models, and follow in detail the results of several Boltzmann-Uehling-Uhlenbeck (BUU) models and quantum molecular dynamics (QMD) models. Concerning pion production, we find a convergence of the codes in the final charged pion yield ratio to a 1σ deviation of about 5%. However, the uncertainty is expected to be reduced to about 1.6% if improved Pauli blocking and calculation of the complex (non-linear) term in the mean-field potential are implemented in all codes.

1. – Introduction

Heavy-ion collisions offer unique possibilities to investigate, in laboratory conditions, nuclear matter away from saturation properties. To this aim, the nuclear states of interest need to be connected to final experimental observables, which is a quite challenging task, leading to information on the Equation of State (EoS). As a matter of fact, transport approaches are the main tool to establish this connection and extract this information. Therefore, the reliability of transport studies of heavy-ion collisions and the robustness of their predictions is important in heavy-ion research. It has recently become apparent that different conclusions could be drawn from the same data by relying on transport simulations, *e.g.*, in the investigations of isospin equilibration in peripheral collisions (isospin diffusion) or in the interpretation of ratios of charged pions, see [1] for a recent review. These discrepancies could naturally derive from the different approximation schemes, adopted in the different transport models, to deal with the quantum many-body problem or from differences in various technical assumptions. The impacts of the numerical details on predictions and conclusions are often difficult to discern. However, a

systematic comparison and evaluation of transport codes under controlled conditions can eventually provide benchmark calculations, thus improving the ability to reach robust conclusions from the comparison of transport simulations with experimental data.

Previous studies along this direction were dedicated to the comparison of transport model predictions for Au + Au collisions [2,3]. The observed differences in the predicted reaction path and corresponding observables (such as collective flows) resulted mainly from differences in the initialization of the systems and in the treatment of the collision integral (Pauli blocking effects). The mean-field dynamics also seemed to play a role. More recently, significant progress in understanding the behavior of the different transport codes was made with subsequent studies, based on box calculations, *i.e.*, simulations of nuclear matter enclosed in a box with imposed periodic boundary conditions [4-6]. In particular, the box calculations have the advantage that the different aspects of heavy-ion collisions can be isolated and tested separately, *e.g.*, the description of N-N scattering processes (*i.e.*, two-body correlations) and the mean-field dynamics. Taking advantage of this background [7], the comparison was then extended to the case of nuclear reactions of experimental interest, focusing on pion observables, as pion ratios turned out to be sensitive indicators of the behavior of the symmetry energy. Here we report on a selection of these recent results [6,8].

2. – Transport approaches

The dynamics of nuclear collisions at Fermi/intermediate energy is usually described by semi-classical transport theories, such as the Nordheim approach, in which the Vlasov equation for the one-body phase space distribution, $f(\vec{r},\vec{p};t)$, is extended with a Pauli-blocked Boltzmann collision term, which accounts for the average effect of the two-body residual interaction. The resulting transport equation is often called Boltzmann-Uehling-Uhlenbeck (BUU) equation. In order to introduce fluctuations and further (many-body) correlations in the treatment of the reaction dynamics, a number of different avenues have been undertaken, which can be differentiated into two classes (see refs. [1,9,10] for recent reviews). One is the class of quantum molecular dynamics (QMD) models [11], while the other kind is represented by stochastic extensions of mean-field approaches of the BUU type [12,13].

2˙1. *BUU-like models.* – In BUU-like approaches, the time evolution of the distribution function, $f(\vec{r},\vec{p};t)$, follows the equation

$$\Big(\frac{\partial}{\partial t}+\vec{\nabla}_p\epsilon\cdot\vec{\nabla}_r-\vec{\nabla}_r\epsilon\cdot\vec{\nabla}_p\Big)f(\vec{r},\vec{p};t)=I_{coll}(\vec{r},\vec{p};t), \tag{1}$$

where $\epsilon[f]$ is the single-particle energy, usually derived from a density functional, and I_{coll} is the (stochastic) two-body collision integral, specified by an in-medium nucleon-nucleon cross section $\mathrm{d}\sigma^{med}/\mathrm{d}\Omega$. The BUU theory can more generally be formulated in a relativistic framework, and actually most codes in our comparison use a relativistic formulation. However, in the simpler non-relativistic representation of the nuclear interaction, the single-particle energy reduces to $\epsilon=\sqrt{\vec{p}^2+M^2}+U(\rho)$ (for the local interactions considered here), where $U(\rho)$ represents the self-consistent mean-field potential. The integro-differential non-linear BUU equation is solved numerically. To this end, the distribution function is represented in terms of finite elements, so-called test particles (TP), characterized by time-dependent centroid coordinates and momenta $\vec{R}_i$

and $\vec{P}_i$. The number of TPs per nucleon is set to $N_{TP} = 100$ in the calculations. Upon this ansatz, the left-hand side of eq. (1) leads to Hamiltonian equations of motion for the TP centroid propagation:

$$\frac{\mathrm{d}\vec{R}_i}{\mathrm{d}t} = \vec{\nabla}_{P_i}\epsilon \qquad \text{and} \qquad \frac{\mathrm{d}\vec{P}_i}{\mathrm{d}t} = -\vec{\nabla}_{R_i}\epsilon. \tag{2}$$

2˙2. *QMD models.* – In QMD models, the many-body state is represented by a simple product wave function of single-particle states with or without antisymmetrization [10, 11]. The single-particle wave functions ϕ_i are usually assumed to have a fixed Gaussian shape:

$$\phi_i(\vec{r}_i;t) = \frac{1}{\left[2\pi(\Delta x)^2\right]^{\frac{3}{4}}} \exp\left[-\frac{[\vec{r}_i - \vec{R}_i(t)]^2}{4(\Delta x)^2}\right] e^{(i/\hbar)\vec{P}_i(t)\cdot\vec{r}_i}. \tag{3}$$

The time evolution of the nuclear dynamics is formulated in terms of the variation of the wave packet centroids, similar to classical molecular dynamics. This strategy yields equations of motion for the coordinates of the wave packets of similar form as obtained for the TPs in BUU. Though the nucleon wave functions are independent (mean-field approximation), the use of localised wave packets induces classical many-body correlations both in the mean-field propagation and two-body in-medium scattering (collision integral), where the latter is treated stochastically. In the philosophy of QMD one wants to go beyond the mean-field approach and include correlations and fluctuations from the beginning. These fluctuations are regulated and smoothed by choosing the parameter Δx, the width of the wave packet, cf. eq. (3). However, being essentially of classical nature, they can lead to a loss of the fermionic character of the system more rapidly than in BUU [4]. The effects of this difference in the amount of fluctuations between the two approaches will clearly be seen in the comparisons that will follow.

3. – Results and discussions

3˙1. *Test of the mean-field propagation.* – A dedicated homework has been devised to test the mean-field propagation under controlled situations in the different transport codes [6]. We consider uniform symmetric matter at saturation density $\rho_0 = 0.16$ fm^{-3} and zero temperature. For the cubic box employed (of size $L_\alpha = 20$ fm), this corresponds to $A = 1280$ nucleons. The system is initialized by impressing a sinusoidal distortion with wave number $k_{ini} = 2\pi/L_\alpha$ and amplitude $a_\rho = 0.2\ \rho_0$ on the density in the box, along the z-direction: $\rho(z, t = 0) = \rho_0 + a_\rho \sin(k_{ini} z)$. The simulations are followed until $t_{fin} = 500$ fm/c, with a recommended time step of either $\Delta t = 0.5$ or 1.0 fm/c. Several BUU-type and QMD-type codes participated in the present comparison [6]. 10 events were considered for the BUU models, whereas 200 events were run for the QMD codes. The Coulomb interaction and the nuclear symmetry force were turned off in this case. For the non-relativistic codes, a standard Skyrme parametrization (without momentum dependence) for the single-particle potential is used, leading to the following nuclear matter properties: compressibility $K_0 = 500$ MeV, saturation density $\rho_0 = 0.16\,\mathrm{fm}^{-3}$ and the binding energy at saturation density $E_0 = -16$ MeV. For the relativistic codes, we employed a non-linear $\sigma-\omega$ Relativistic Mean Field (RMF) parameterization, characterized by the same properties. The nucleon mass was taken to be $M = 938$ MeV. To characterize the density perturbation introduced in the initial conditions and its time evolution, it

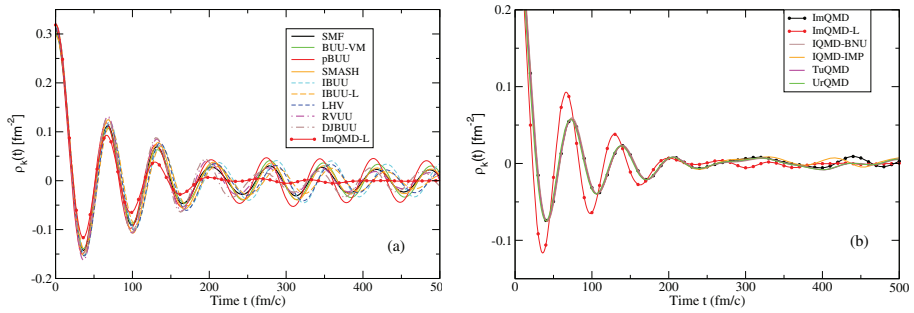

Fig. 1. – (Color online). The strength function $\rho_k(t)$ for mode k_{ini} is displayed as a function of time. Results are shown for BUU-like calculations (left panel), including ImQMD-L calculations for comparison, and QMD-like calculations (right panel) (adapted from ref. [6]).

is useful to perform a Fourier analysis of the density oscillations. We define the Fourier transform of the averaged spatial density as $\rho_k(t) = \int_0^{L_z} \mathrm{d}z\, \rho(z,t)\, \sin(kz)$, which can be called the strength function of the mode k. We will consider $k = k_{ini} = 2\pi/L_\alpha$. One generally observes damped oscillations as a function of time for the latter quantity.

Figure 1 shows the results obtained for the time evolution of the strength function, for all codes involved in the comparison. One can observe that BUU-like codes give quite similar results. The differences observed are compatible with the different formalism (either fully covariant, non-relativistic or with only relativistic kinematics) adopted in the different models. The QMD-like codes exhibit an excellent agreement among them, but a lower oscillation frequency and larger damping effects are observed with respect to the results of BUU-like codes. This observation highlighted relevant effects of the approximate treatment of the many-body term of the nuclear interaction in QMD [14], resulting in the lowering of the oscillation frequency. A more accurate treatment is found in recent formulations (see in particular the ImQMD-L code) adopting the Lattice Hamiltonian method to implement the mean-field dynamics [14], that leads to a better agreement with the BUU-like results, as also shown in the figure.

3˙2. *Comparison of nuclear reaction dynamics and pion production.* – The comparison was then extended to the dynamics of a nuclear reaction, including meson (pion) production. Thus, in this homework calculation, we incorporate inelastic collisions related to the production of pion-like particles. We consider the reaction ^{132}Sn+^{124}Sn at the incident energy 270 AMeV and an impact parameter $b = 4$ fm. A common initialization was adopted for all participant codes. A simple (momentum-independent) parametrization was used for the mean-field potential, leading to the saturation density $\rho_0 = 0.16\,\mathrm{fm}^{-3}$, the binding energy at saturation density $E_0 = -16$ MeV, the incompressibility of symmetric nuclear matter $K_0 = 240$ MeV, the symmetry energy at saturation density $E^0_{sym} = 30.3$ MeV, and its slope parameter at saturation density $L = 84$ MeV. Simulations are carried out until $t = 70\,\mathrm{fm}/c$ and 100000 events were considered.

Results from full-mode calculations, *i.e.*, including mean-field propagation and n-n collisions, for both BUU and QMD models are displayed in fig. 2. Comparing BUU and QMD models, a substantially stronger flow is seen for BUU. This is consistent with the fact that BUU models lead to a lower density as a result of the stronger repulsion of the accurately calculated non-linear force, see also the results discussed in the previous

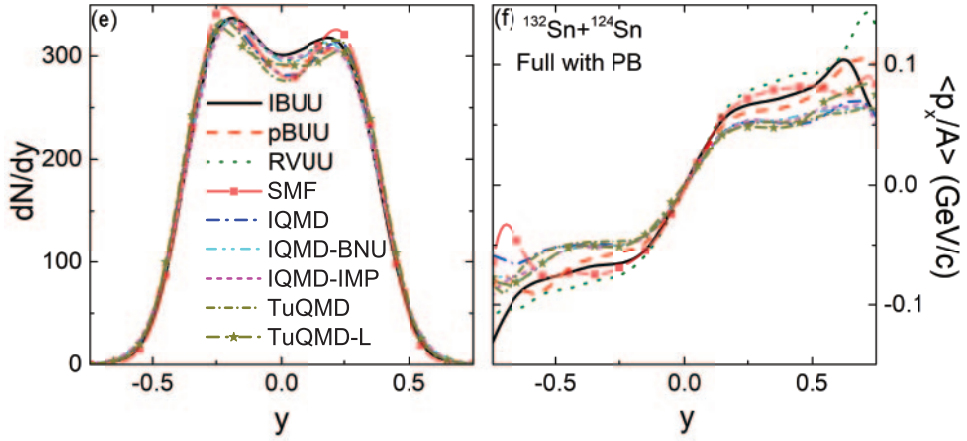

Fig. 2. – (Color on line). Final nucleon rapidity (e) and transverse flow (f) distributions for all codes in their standard implementations and with standard parameters (adapted from ref. [8]).

subsection. This difference is further enhanced by the use of an effectively larger particle size in QMD, which reduces the gradients of the mean-field potential. The differences within BUU models also follow from the same connection that a smaller TP size leads to a stronger force and thus to a stronger stopping and flow. Indeed, using the point TP, RVUU has the largest flow and a large stopping. QMD models in the standard versions agree well among themselves, especially for the transverse flow. The agreement with BUU results can be improved by using a more elaborate lattice formulation for QMD. Since pion production in heavy-ion collisions is sensitive to the evolution of the nucleonic matter through the reached densities and asymmetries, and consequently to the rate of isospin-dependent NN collisions, we have to expect also differences in pion observables.

The final π^-/π^+ yield ratios from different simulation modes for all participant codes are compared in fig. 3. We first discuss the ratios in the Cascade mode (*i.e.*, suppressing the mean-field propagation) in the left panel. The small differences in the π^-/π^+ yield

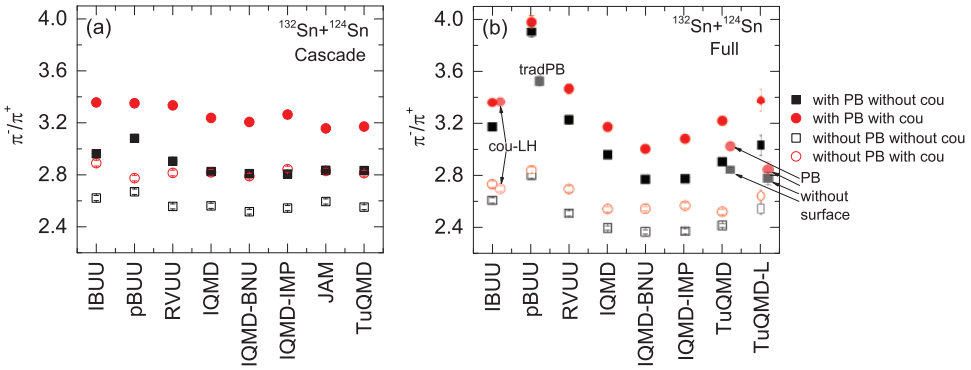

Fig. 3. – (Color online). π^-/π^+ yield ratios in different scenarios (see legend and text) for BUU-like (left) and QMD-like (right) codes (from ref. [8]).

ratio in the Cascade mode without Pauli blocking and Coulomb potential (open black symbols) are consistent with those seen in the corresponding box calculation in ref. [5]. Including the Coulomb potential increases the ratios strongly, since the Coulomb force pushes out the protons and makes the high-density region more neutron-rich. With the use of a width parameter of $\Delta x = 1.41$ fm, the QMD codes have similar Coulomb effects as IBUU and RVUU with their default cut-off parameters. With isospin-dependent Pauli blocking included for nucleons (solid symbols), the π^-/π^+ yield ratios are significantly increased, consistent with the fact that the $pp \to n\Delta^{++}$ reaction, which leads to π^+ production, is more blocked than the $nn \to p\Delta^-$ reaction, which leads to π^- production. We note that generally one expects an anti-correlation between the pion yield and the charged pion yield ratio, since with larger pion yields, differences between the charge states become less important. BUU models with a stronger Pauli blocking generally give a larger π^-/π^+ yield ratio compared with QMD models, and this is particularly true for pBUU with a more effective Pauli blocking. Turning on the Coulomb potential leads to a similar increase of the π^-/π^+ yield ratio. As a whole, the pion ratios are rather consistent among all models in the Cascade mode, with the exception of pBUU which has a rather small Coulomb effect with and without Pauli blocking. Differences in the π^-/π^+ yield ratio among models become larger after the inclusion of mean-field potentials, as seen in panel (b) of fig. 3. A systematically larger π^-/π^+ yield ratio is seen for BUU models compared with QMD models, already in the Full-noPauliBlocking (nopb) mode and more pronounced with Pauli blocking included. This is related to the lower total pion multiplicity in BUU models compared with QMD models, as a result of the stronger force and the lower densities reached in BUU models. For QMD models, the π^-/π^+ yield ratios are similar among codes that use the traditional method for the mean-field calculation. We also show a lattice calculation with TuQMD (TuQMD-L), which gives a larger π^-/π^+ yield ratio compared to other QMD models, related to the smaller total pion yield([1]). Generally, the π^-/π^+ yield ratios are increased after incorporating the Coulomb potential. With the inclusion of the isospin-dependent Pauli blocking, the π^-/π^+ yield ratios are further increased, especially in pBUU among BUU models and in IQMD and TuQMD among QMD models. The higher π^-/π^+ yield ratios for TuQMD and IQMD are due to the use of the surface correction to the Pauli blocking, which reduces the pion yields and thus increases the π^-/π^+ yield ratios, making them comparable to those from the IBUU and RVUU codes. It is remarkable to see the good agreement between TuQMD-L calculations with the surface correction on the Pauli blocking and the results of IBUU and RVUU (full red circles in the figure). The large charged pion yield ratio for pBUU is related to the fact that in this code pions and Δ resonances are subject also to the symmetry energy in contrast to all other codes, unlike the setup in the homework specifications. Thus, the results of this code are not really comparable to the other codes.

4. – Conclusions

Here we report on a study of mean-field dynamics in a box, without collisions, and of the full dynamics of a nuclear reaction, including pion production. Major transport codes from the two basic families, BUU and QMD, are included in this study, which

([1]) The TuQMD-L results show a larger error bar of about 6% compared to others, since these were obtained from a time-consuming calculation with a considerably smaller number of events.

also partly account for relativistic effects in different approximations. The comparisons include the strength function characterizing mode evolution in mean-field dynamics and several observables related to reaction dynamics at intermediate energies. We find that we can generally understand consistencies and differences between the results of the different codes. The remaining differences among codes and relative to near-exact results include: 1) approximations to the calculation of the non-linear terms of the force used in QMD codes that lead to noticeable differences in the frequency of the density oscillations even at early times. This can, however, be avoided in a lattice evaluation scheme; 2) the fluctuations inherent in the coarse phase space representation (and consequent Pauli-Blocking evaluation), which are characteristically different in BUU and QMD codes. It should be noticed that these findings do not make a statement about the validity of the two approaches, since the physical modeling is different: QMD codes attempt to put a reasonable amount of fluctuations already into the ansatz for the many-body state representation, while in BUU these would have to be included by an extra fluctuation term in the Langevin framework. A dedicated comparison of the fluctuation dynamics in the two families of approaches is foreseen. However, the agreement within 5% observed in our comparison for pion ratios gives good confidence about the reliability of this observable to extract constraints on the symmetry energy, as considered in recent analyses [15], which also combine constraints from nuclear structure and astrophysical scenarios [16, 17].

REFERENCES

[1] Colonna M., *Prog. Part. Nucl. Phys.*, **113** (2020) 103775.
[2] Kolomeitsev E. E. *et al.*, *J. Phys. G*, **31** (2005) S741.
[3] Xu J. *et al.*, *Phys. Rev. C*, **93** (2016) 044609.
[4] Zhang Y. *et al.*, *Phys. Rev. C*, **97** (2018) 034625.
[5] Ono A. *et al.*, *Phys. Rev. C*, **100** (2019) 044617.
[6] Colonna M. *et al.*, *Phys. Rev. C*, **104** (2021) 024603.
[7] Wolter H. *et al.*, *Prog. Part. Nucl. Phys.*, **125** (2022) 103962.
[8] Xu J. *et al.*, *Phys. Rev. C*, **109** (2024) 044609.
[9] Xu J., *Prog. Part. Nucl. Phys.*, **106** (2019) 312.
[10] Ono A., *Prog. Part. Nucl. Phys.*, **105** (2019) 139.
[11] Aichelin J., *Phys. Rep.*, **202** (1991) 233; *Phys. Rev.*, **33** (1986) 537.
[12] Ayik S. and Gregoire C., *Phys. Lett. B*, **212** (1988) 269; *Nucl. Phys. A*, **513** (1990) 187.
[13] Danielewicz P., *Nucl. Phys. A*, **673** (2000) 375; Danielewicz P. and Bertsch G. F., *Nucl. Phys. A*, **533** (1991) 712.
[14] Yang J. *et al.*, *Phys. Rev. C*, **104** (2021) 024605.
[15] Estee J. *et al.*, *Phys. Rev. Lett.*, **126** (2021) 162701.
[16] Tsang C. Y. *et al.*, *Nat. Astron.*, **8** (2024) 328.
[17] Huth S. *et al.*, *Nature*, **606** (2002) 276.